Available online at www.sciencedirect.com
SCIENCE DIRECT®
Earth and Planetary Science Letters 245 (2006) 315–329
EPSL
www.elsevier.com/locate/epsl

Asymmetric rifts due to asymmetric Mohos: An experimental approach

Giacomo Corti *, Piero Manetti

Istituto di Geoscienze e Georisorse (IGG), Consiglio Nazionale delle Ricerche (CNR), via G. La Pira 4, 50121 Firenze, Italy

Received 11 August 2005; received in revised form 26 January 2006; accepted 3 February 2006
Available online 11 April 2006
Editor: V. Courtillot

Abstract

Large-scale asymmetries in structures, and in the uplift, width and volcanism of pairs of conjugate passive margins have been documented in various parts of the world; these asymmetries reflect the dominant mode of extension preceding the break-up of the continental lithosphere. Of the many parameters involved, the pre-rift crustal structure has been shown to play a fundamental role in controlling the process of continental rifting. In this work, we have used analogue models to show how initial asymmetric Moho configurations are prone to produce asymmetric rifting, with prominent asymmetries in the amount of extension accommodated by boundary faults, in the patterns of lithospheric thinning/asthenospheric upwelling, and in the trajectories of magma migration. After continental break-up, these deformative patterns are expected to lead to the development of a pair of asymmetric passive margins, with one narrow, strongly volcanic margin and a wider, less volcanic (or with areas of concentrated volcanic activity) counterpart.

Keywords: continental rifting; analogue modelling; rift asymmetry; passive margins; pre-rift crustal structure

1. Introduction

Passive margins are the result of extension of the continental lithosphere, its break-up and the opening of an oceanic basin. Many geophysical evidences from passive margins worldwide suggest that large-scale asymmetries are the final product of continental rifting (Fig. 1) (e.g., [1–4]). These asymmetries, expressed in different patterns of volcanism, in the width, uplift, subsidence, and thickness of sediments, in the amount of extension accommodated prior to rupture of the lithosphere, as well as the location and timing of the initiation of seafloor spreading (e.g., [4–7]), reflect the dominant mode of extension preceding break-up and the onset of seafloor spreading. As a consequence, asymmetric margin pairs have been widely referred to models involving a lithospheric-scale simple shear deformation [8], as compared to the pure shear symmetric model [9] in which the lithosphere is uniformly thinned during rifting. Besides these kinematic models, several parameters have been proposed to control the continental rifting process and the variability in passive margin characteristics, including among others: the rheological or thermal structure of the lithosphere (e.g., [10,11]); the presence of a pre-rift lithospheric structural grain and inherited weakness zones [3,12–18]; the melt volumes at a margin [19]; migration of extension due to cooling and hardening of the stretched lithosphere (e.g., [20–23]),

* Corresponding author. Tel.: +39 055 2757528; fax: +39 055 290312.
E-mail address: cortigi@geo.unifi.it (G. Corti).

0012-821X/$ - see front matter © 2006 Elsevier B.V. All rights reserved.
doi:10.1016/j.epsl.2006.02.004

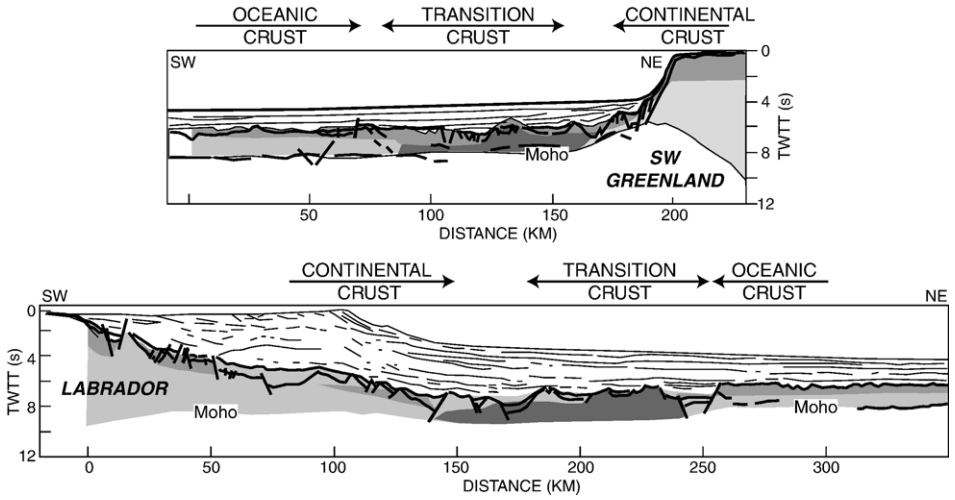

Fig. 1. Multichannel seismic reflections on the conjugate margins of the Labrador Sea showing the difference in lateral extent of the zone of stretched continental crust between the narrow Greenland margin (thinned zone width ~70 km) and the wide Labrador margin (thinned zone width ~140 km). After [1].

eventually leading to break-up at one side of a wide rift (e.g., [24]); the development of small-scale convection enhancing heating and weakening of the lithosphere (e.g., [1]); the kinematics of extension (orthogonal vs. oblique; [3]); the westward drift of lithosphere relative to the underlying mantle [25]; strain-softening processes [26]; mantle serpentinization [27] and the decoupling of upper crustal and mantle deformation, which is in turn controlled by crustal rheology [28]. A combination or sequence of the above-mentioned processes is likely to contribute to the observed asymmetry of passive margins.

Dunbar and Sawyer [12–14] were among the first to make a detailed study of the control exerted by the inherited structural grain on the continental break-up process and the geometry of the resulting passive margins. These authors suggested that rupture of the continental lithosphere is far more likely to occur when the extensional structures follow the pre-existing structural grain; in these conditions, the pre-rift Moho topography may have a crucial influence on the continental break-up process. Indeed, by replacing the strong lithospheric mantle material with weak crustal material, a local increase in thickness of the crust is expected to strongly reduce the integrated resistance of the lithosphere. As a consequence, lateral variations in crustal thickness are able to strongly control rifting and the geometry of the resulting margins pair, as supported by numerical modelling [29].

In our work, we have analysed this hypothesis by means of scaled analogue models, showing that extension-parallel pre-rift Moho asymmetries may lead to a lithospheric-scale asymmetry in the rifting process and in the resulting pair of passive margins.

2. Experimental modelling

We performed a series of 18 analogue experiments simulating the extension of a three-layer continental lithosphere (upper and lower crust, lithospheric mantle) floating above a fluid-like material representing the asthenosphere (Fig. 2) (e.g., [29,30]). The models were deformed in an artificial gravity field of 15 g using the large-capacity centrifuge at the Tectonic Modelling Laboratory of CNR-IGG, hosted by the Department of Earth Sciences, the University of Florence (Fig. 2a–c). During the experiments, the models underwent vertical thinning and lateral expansion in response to the centrifugal forces. Gradual removing of rectangular Plexiglas blocks (spacers) during successive runs in the centrifuge allowed control of the extension velocity (Fig. 2d) [29]. With this set-up, the centrifuge forces exerted a uniform stress field on the models and the different distribution of deformation was imposed only by lateral variations in rheology and in the strength of the analogue layers. These conditions are a reasonable approximation of the natural process of extension of the continental lithosphere at a regional scale.

2.1. Model rheology and materials

Following Dunbar and Sawyer [12–14], the models were aimed to investigate the extension of a continental lithosphere characterised by a pre-existing structural

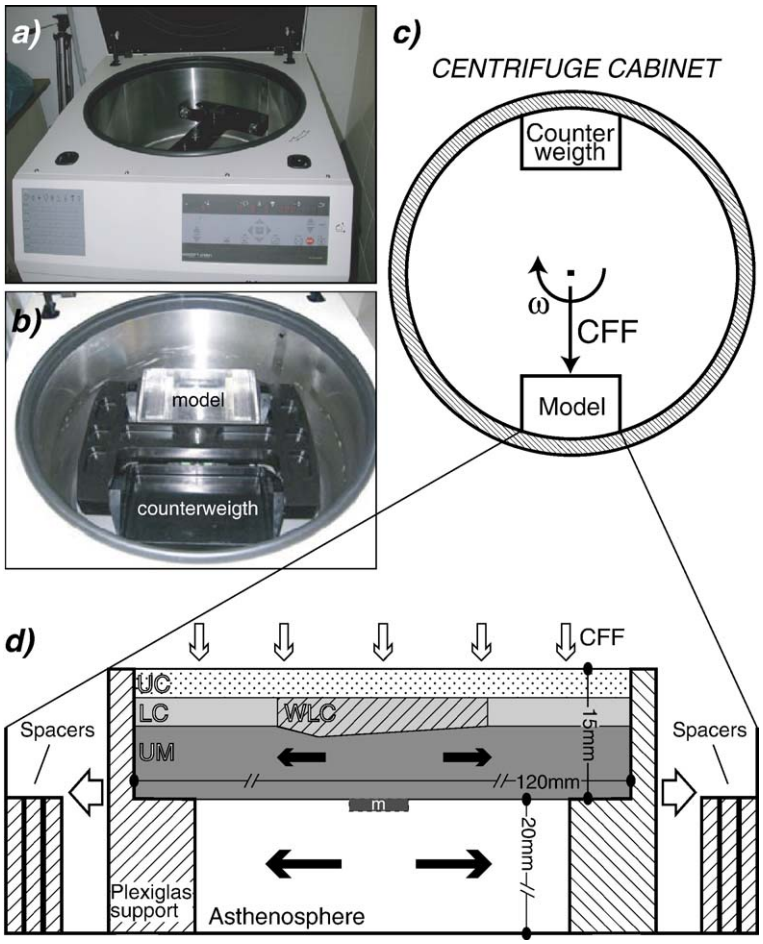

Fig. 2. Sketch of the experimental set-up. a) Lateral photo of the centrifuge apparatus; b) close up of the internal rotor; c) schematic representation of the centrifuge cabinet showing loading conditions in centrifuge; ϖ is the angular velocity, CFF is the centrifuge force field. d) Model set-up and rheological stratification. Removal of rectangular Plexiglas spacers allows the models, under the centrifuge force field, to collapse and fill the empty space. The velocity of lateral flow of the asthenosphere is higher than that of the lithosphere (see black arrows); as a result, the Plexiglas supports are moved apart and pull the model lithosphere. As in natural conditions, extension is a combination of drag at the base of the lithosphere due to flow of the model asthenosphere and far field extensional forces acting from the lateral boundaries of the models. LC: lower crust; m: analogue melt; UC: upper crust; UM: upper lithospheric mantle; WLC: weak lower crust.

grain. Most of the major Mesozoic and Cenozoic rift systems are, in fact, not randomly distributed but tend to follow the trend of Pan African, Caledonian, Hercynian and Alpine orogens, avoiding cratonic regions (e.g., [3,12,31]). This results from weaker rheology of Late Precambrian or Phanerozoic mobile belts with respect to the adjacent old craton [32]. In nature, the pervasive rheological heterogeneities that lead to a weakening of continental masses generally locate within the crust, the upper mantle or spread throughout the lithosphere (e.g., [3]). Within the pre-deformed regions lateral variations in lower crustal rheology are expected to reduce the total strength of the lithosphere (e.g., [12,33]); these pervasive rheological heterogeneities, leading to strain localisation and controlling both rift location and its structural pattern, have been simplified in our models by introducing a weakness zone in the lower crust (WLC; [29]).

In the models, K-feldspar sand simulated the upper brittle crust; a ductile mixture of silicone and corundum sand reproduced the “normal” lower crust whereas a less viscous (i.e., weaker) mixture of silicone, sand and oleic acid was used to reproduce the inherited weakness zone (WLC). A denser and stronger silicone–sand mixture simulated the lithospheric mantle; below this layer a low-viscosity silicone–sand–oleic acid mixture simulated the asthenosphere, providing isostatic support to the deforming lithosphere with a free-slip boundary at the bottom of the ductile mantle. Glycerol was used to simulate sub-lithospheric melts. The characteristics of the various materials are reported in Table 1.

Table 1
Characteristics of experimental materials for the different series

Analogue Material	Prototype layer	Density (kg m^{-3})	Coefficient of internal friction	Cohesion (Pa)	Rheological characteristics	Power-law parameters
K-Feldspar sand ($)	Upper crust	1220 (±10)	μ ~ 0.6	80	Brittle	
Silicone (§)+corundum sand (∧) (100:30; % in weight)	Lower crust	1260 (±10)			Power-law	n=1.25 A=4 10^{-6} (*)
Silicone (§)+corundum sand (∧)+oleic acid (100:30:15; % in weight)	Weak lower crust	1230 (±10)			Power-law	n=2.30 A=6 10^{-7} (*)
Silicone (§)+corundum sand (∧) (100:50; % in weight)	Upper mantle	1415 (±10)			Power-law	n=1.35 A=1 10^{-6} (*)
Silicone (§)+corundum sand+oleic acid (100:60:30; % in weight)	Asthenosphere	1400 (±10)			Power-law	n=1.70 A=4 10^{-3} (*)
Glycerol	Magma	1260 (#)			Newtonian	η=1 Pa s (#)

($) Dry K-Feldspar sand with angular grains with dimension ~200 μm.
(§) Mastic Rebondissante 29 (produced by CRC France).
(∧) Dry Corundum sand with rounded grains with dimension <250 μm.
(*) Measured with a coni-cylindrical viscometer at room temperature (20 °C±1°).
(#) After Cruden et al., 1995.

2.2. Types of model

Three different experimental series were performed in order to investigate the effect of lateral variations in the pre-rift Moho topography on continental break-up. In the models, we tested crustal thickness variations within the WLC only, as the crustal roots inducing the Moho depressions in nature are expected to occur below the weak orogenic belts localising rifting.

The Type 1 model presented a WLC of uniform thickness; this reference model was thus characterised by an inherited low-strength region with a symmetrical, rectangular geometry.

In the Type 2 models, the thickness of the WLC was varied laterally in order to create an initial asymmetric crustal configuration caused by the presence of a lateral crustal root (Fig. 2d). The Moho thickness within this root was increased by 15% to 40% with respect to adjacent regions in different experiments, as hypothesized for the pre-rift structure in the North Atlantic passive margins [7,13,16]. This set-up induced lateral variations in the integrated lithospheric resistance, the strength of the lithosphere in correspondence to the thickest WLC being from 10% to 25% lower than in adjacent regions; in nature, the reduction in strength of the weakened lithosphere has been estimated at up to 50% (e.g., [13]).

All the Type 1 and 2 models were characterised by similar rheological layering, whereas a series of models (Type 3) reproduced the presence of sub-lithospheric melts during extension (Fig. 2d). This third series of experiments was designed to investigate the trajectories of melt migration during rifting; these boundary conditions could represent an advanced stage of rifting stage or plume-dominated extensional processes in which deep, hot mantle material is channelled below ancient orogenic belts [34], triggering partial melting below the weak lithospheres and the occurrence of voluminous flood basalt volcanism before significant lithospheric extension has occurred (e.g., [35]). This process may ultimately lead to the development of volcanic rifted margins (e.g., [36]). Other initial boundary conditions (e.g., kinematics of extension, strain rate) were the same in all the experiments performed, so differences in rift evolution were expected to be caused by the prescribed Moho configuration.

2.3. Scaling

The models were scaled to natural conditions using a geometrical scaling ratio of ~1.7 10^{-7} (1 mm in the models simulated ~5 km in nature), so that we modelled the extension of a continental lithosphere of ~80 km thickness (e.g., [3]). Dynamic-kinematic similarity ensured that the velocity of extension in the models scaled to natural values of ~10 mm yr^{-1}, a reasonable value for rift systems (e.g., [3]). Details of scaling are reported in Appendix A, supplementary data.

2.4. Simplifications of modelling

Analogue modelling is a simplification of the natural continental extension process, mainly in terms of rheological and thermal boundary conditions. Particularly, the continental lithosphere has been schematised to a three-layer brittle/ductile system, with a highly simplified rheology characterising each single layer (e.g., [37]). For instance, both viscous and frictional properties have been modelled as invariant with depth and temperature-

independent. In addition, these layers were considered homogenous at the scale of the investigated process, although in nature discrete pre-existing discontinuities inherited from previous tectonic phases may influence the formation of structures at lithospheric scale. Both lateral and vertical boundaries between the different crustal and/or mantle layers (e.g., model Moho, lateral boundary between the normal and weak lower crust) were sharp discontinuity in the experiments, whereas in nature they normally occur as complex and variable transition zones (e.g., [3]). The current models did not properly reproduce thermal conditions (e.g., vertical thermal gradient, temperature variations during progressive extension), nor chemical or petrological variations occurring during rifting. This prevented rheological modifications in the different layers and destabilization of both the brittle–ductile transition in the crust and the Moho discontinuity, which continuously evolve during lithospheric thinning (e.g., [3]). Finally, syn-extension surface processes as erosion and sedimentation were not considered during the experiments, although these processes have been shown to have an influence on the extensional basin evolution (e.g., [38,39]).

Despite these simplifications, the current analogue models were able to trace the large-scale response to extension of the continental lithosphere and allowed to analyse the effects of the initial Moho topography on the rifting process (see below).

3. Experimental results

The modelling results are presented through discussion of three different models representing the entire set of experiments. In fact, all the models showed similar deformation in terms of evolution of structures and patterns of lithospheric thinning/asthenospheric upwelling.

3.1. Evolution of deformation

In the symmetric (Type 1) model (i.e., no lateral variations in crustal thickness), the WLC localised deformation, leading to the development of a pair of boundary fault systems (Fig. 3). Both fault systems developed at low extension values (bulk extension ~4%); as extension increased, part of the deformation shifted within the main depression, with development of pervasive, closely spaced faults with limited vertical displacement (internal faulting; Fig. 3). At the end of model deformation, both boundary fault systems were characterised by prominent fault scarps, testifying to a first-order symmetry in the amount of extension accommodated by the conjugate border faults (Figs. 3, 4).

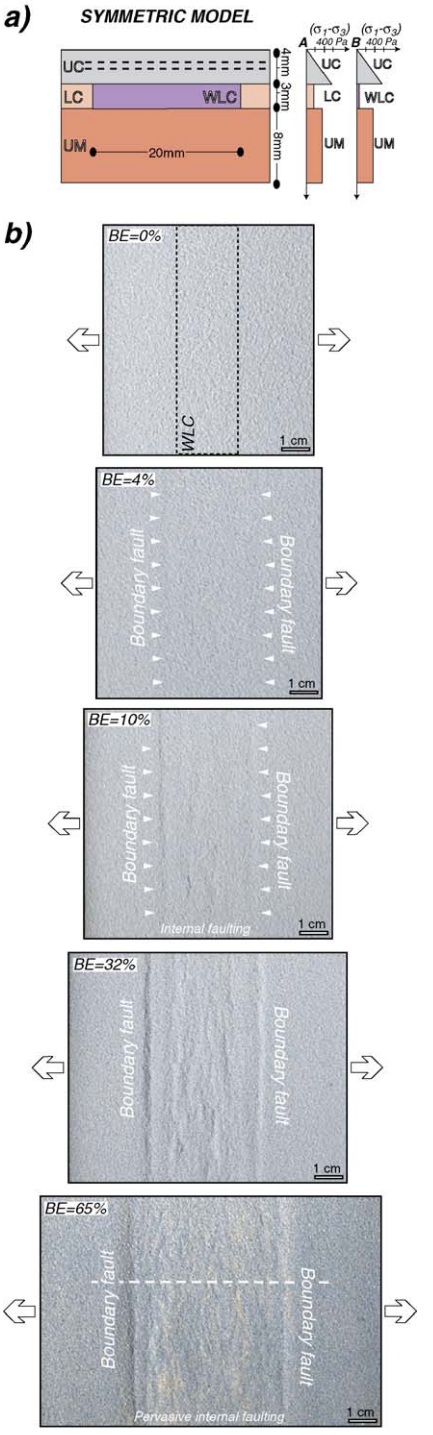

Fig. 3. a) Rheological layering of symmetric model RWZR19 (uniform crustal thickness of 7 mm; bulk extension: 65%) and model strength profiles (see Appendix 1 for details of calculations). b) Top-view photos showing the progressive deformation of the model (light is from left to right). BE: bulk extension; WLC: weak lower crust. Other abbreviations as in Fig. 2. White dashed line indicates the trace of the cross-section of Fig. 4a.

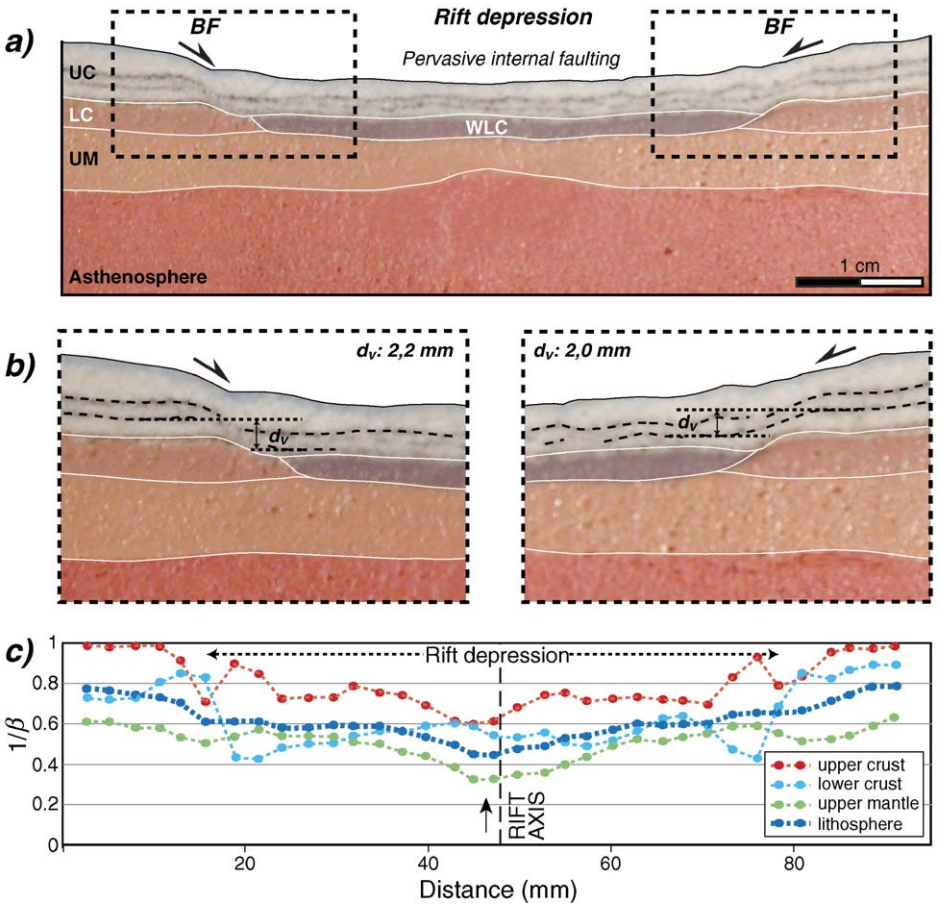

Fig. 4. a) Longitudinal cross-section of symmetric model RWZR19 (trace indicated in Fig. 3). BF: boundary fault systems. Other abbreviations as in Fig. 2. b) Close up of the rift margins structure, showing the similar vertical displacement (d_v) along the boundary faults. c) Crustal, mantle and lithospheric thinning factors expressed as $1/\beta$ ratio (i.e., ratio between the initial and final thickness of each layer). Low values of $1/\beta$ indicate high lithospheric thinning and vice versa. Dark arrow indicates the area of maximum lithospheric thinning. Note that both the ductile lower crust and upper mantle are characterised by $1/\beta<1$ (i.e., thinning) along their entire length, indicating that viscous deformation of these layers was not restricted to the region corresponding to the rift at the surface. See text for details.

In Type 2 models, with an initial asymmetric Moho profile, the WLC localised deformation and faulting; however, extension led to enhanced strain in the areas of thickest WLC (Fig. 5). As a result, extension was at first accommodated by the development of a major boundary fault system (MBF) in correspondence to the deepest Moho (Fig. 5); a minor normal fault system (mBF) nucleated on the opposite side of the WLC for increasing amount of bulk extension only. Both faults increased their throw for progressive deformation, accommodating basin subsidence (Fig. 5). At ~30% bulk extension, deformation was partly accommodated by internal faulting; increased extension led to further basin subsidence and to localization of internal faulting in correspondence to the area of initial thickest WLC, where marked thinning of the upper crust occurred (Fig. 5, bulk extension 65%). The MBF was characterised by the most prominent fault scarp on the model surface, testifying to an asymmetry in the amount of extension accommodated by the conjugate border faults.

3.2. Model cross-sections

Analysis of cross-sections of the symmetric model (Fig. 4) emphasizes the first-order symmetry in the extension-related structures at both upper crustal and lithospheric/asthenospheric scales. In the upper crust, extension was accommodated by slip along the boundary faults and development of closely spaced normal faults with limited vertical displacement that pervasively deform the brittle layer (referred to as pervasive internal faulting). The major fault systems nucleated at the WLC boundaries and rooted within the ductile lower crust. Extensional deformation was uniformly accommodated

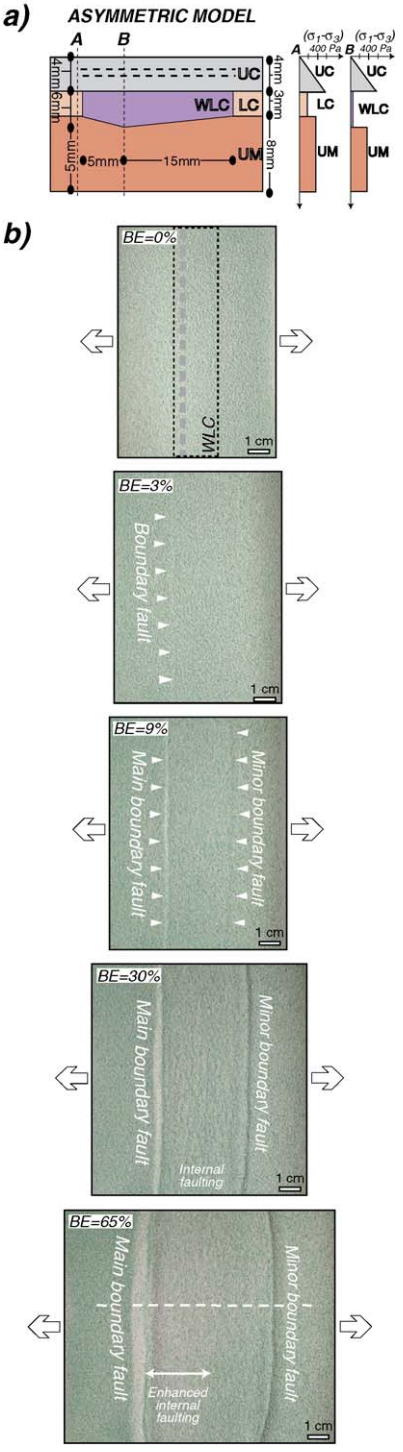

Fig. 5. a) Rheological layering of asymmetric model RWZR16 (crustal thickness: 7 mm; maximum crustal thickness: 10 mm; bulk extension: 65%) and model strength profiles. b) Top-view photos showing the progressive deformation of the model (light is from right to left). The grey dashed line indicates the region with thickest crust. BE: bulk extension; WLC: weak lower crust. Other abbreviations as in Fig. 2. White dashed line indicates the trace of the cross-section of Fig. 6a.

by the two border fault systems, as revealed by the comparable vertical displacements d_v (Fig. 4b). This resulted in a similar relative uplift of the basin margins and maximum basin in the centre of the rift depression (Fig. 4). In the lower crust and upper mantle, extension was taken up by ductile deformation that was not restricted to the width of the rift at the surface but was distributed across the model. Maximum thinning of these layers occurred in the centre of the rift depression (at the rift axis), where maximum asthenospheric upwelling was observed (Fig. 4b,c).

Conversely, cross-sections of the Type 2 asymmetric models (Fig. 6) display a marked asymmetry in extension-related structures. Within the upper crust, deformation was not uniformly distributed across the model, the vertical displacement (d_v) on the MBF being about twice as high as that on the mBF (Fig. 6); this also resulted in a larger relative uplift of the MBF margin with respect to the opposite margin and a maximum basin subsidence in correspondence to the deepest Moho. Similarly, the lower lithosphere/asthenosphere system displayed a strong asymmetry in the pattern of deformation. Lithospheric thinning was laterally inhomogeneous, with maximum values occurring close to the MBF, in correspondence to the initial deepest Moho (Fig. 6c); this area also corresponded to the maximum asthenospheric upwelling, which thus occurred in a lateral position with respect to the rift axis. A relative maximum of the lithospheric thinning was observed close to the mBF margin (Fig. 6c). Comparison of different models suggests that the asymmetric features outlined above increased as the amount of total extension increased. In particular, increasing the bulk extension was seen to lead to a general increase in both absolute values of d_v and in the difference in displacement between the major and minor boundary faults (Fig. 7a). Similarly, the lithospheric thinning and the distance between the region of maximum asthenospheric upwelling and the rift axis also increased when increasing extension (Fig. 7b).

Model strength profiles superimposed on the final longitudinal cross-section (Fig. 8) illustrate the substantial lateral variations in the mechanical strength of the model lithosphere induced by the differential thinning of the analogue crustal and mantle layers (e.g., [40]). This analysis indicates that the strength minimum in the extended lithosphere occurs in the centre of the rift in Type 1 symmetric model. Conversely, in models with initial asymmetric Moho profile, the strength minimum occurs close to the MBF, in correspondence to the initial weakest parts of models (i.e., thickest WLC); a subordinated

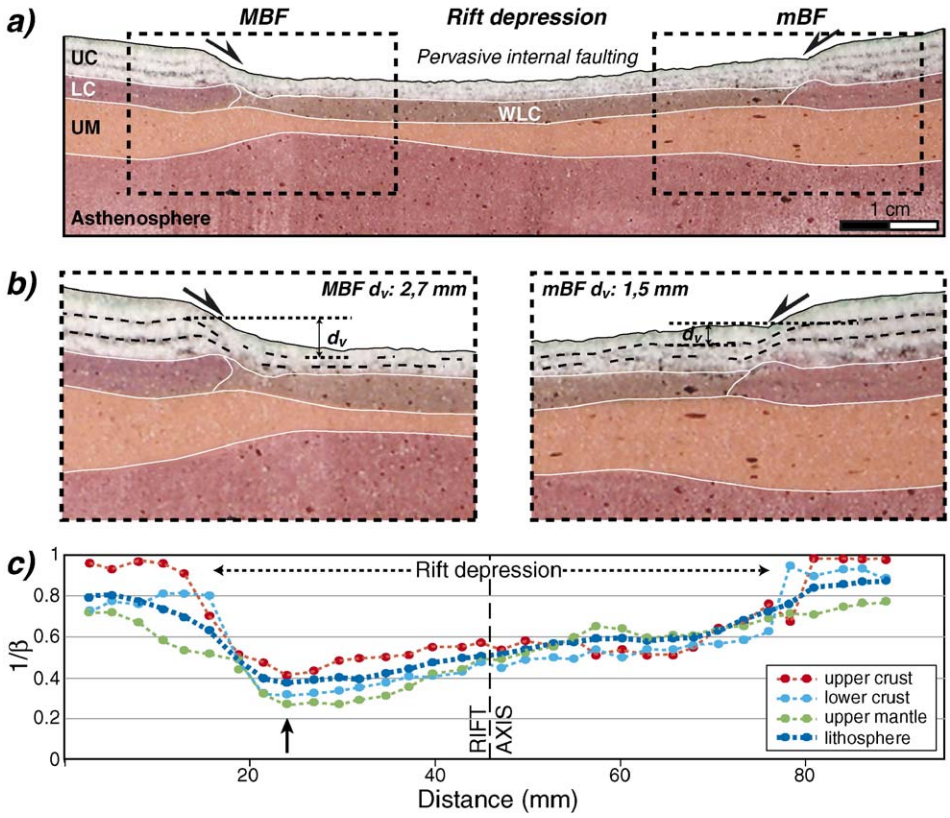

Fig. 6. a) Longitudinal cross-section of asymmetric model RWZR16 (trace indicated in Fig. 5). MBF: major boundary fault system; mBF: minor boundary fault system. Other abbreviations as in Fig. 2. b) Close up of the rift margins structure, highlighting the strong differences in the vertical displacement (d_v). c) Crustal, mantle and lithospheric thinning factors. Dark arrow indicates the area of maximum lithospheric thinning. See text for details.

minimum characterises the mBF. At its minimum value, the integrated lithospheric strength is reduced by more than 3 times relative to the initial configuration, suggesting that rupture of the model lithosphere is expected to occur in the areas of initially thickest Moho, well away from the centre of the rift depression.

3.3. Trajectories of analogue melt migration

Asymmetric models simulating an initial sub-lithospheric magmatic underplating (Type 3; Fig. 9) displayed an analogous, asymmetric evolution of structures with a MBF developing in correspondence to the deepest Moho. As observed for the preceding models, the cross-section (Fig. 9) shows asymmetry in fault displacement, margin uplift and asthenospheric upwelling. Moreover, although the position of the analogue melt was not pre-determined, being located in the centre of the future rift zone, the asymmetric rifting induced by the initial Moho configuration led to a strong asymmetry in the melt migration trajectories. Indeed, the final major accumulation occurred below the area of initial deepest Moho, and the region affected by underplating encompassed the MBF rift margin, where prominent off-axis analogue magma emplacement was also observed (Fig. 9).

4. Discussion and implications for the natural process of continental break-up

4.1. Asymmetric rifts due to asymmetric Mohos

Analogue models have proved to represent valuable tools for investigating the complex strain patterns associated with continental rifting, break-up and the development of conjugate margins (e.g., [11]). Many of these models (e.g., [41–43]) considered symmetric initial boundary conditions with no lateral variations in rheology. Experiments have shown that extension resulted in a symmetric lithospheric-scale deformation superimposed onto complex strain patterns and shear

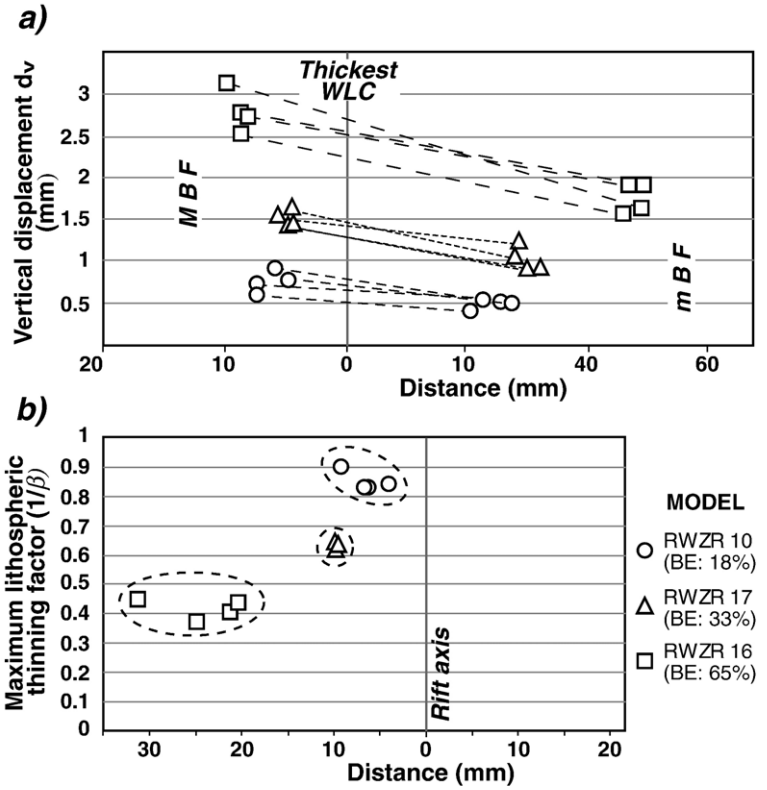

Fig. 7. a) Variation in vertical displacement (d_v) on conjugate border fault pair plotted against the distance from the region of thickest weak lower crust (WLC) in models with different bulk extension (BE). Higher d_v values (left side) correspond to the major boundary faults (MBF), whereas lower d_v values (right side) correspond to the minor boundary faults (mBF). Note that the maximum values of d_v corresponding to the MBF always occur on the rift margin developing in correspondence of the deepest Moho; also note that both absolute values of d_v and the difference in displacement between the major and minor boundary faults increase increasing the bulk extension. b) Plot of the maximum lithospheric thinning factors ($1/\beta$) as a function of the distance from the rift axis. In the different models, maximum thinning occurred away from the rift axis, in correspondence of the thickest WLC. Note that the distance between the region of maximum thinning and the rift axis increases increasing the bulk extension. All the models have normal crustal thickness of 6 mm and maximum crustal thickness of 10 mm.

zones developing at rheological interfaces [42]; the progressive evolution of these shear zones may lead to either symmetric or asymmetric rifting [43]. Models involving the presence of weakness zones within the extending lithosphere [29] have shown that these weaknesses favour rapid necking of the model lithosphere; with symmetric initial boundary conditions (e.g., no lateral variations in crustal thickness; Type 1 symmetric model), the rifting process is symmetric at lithospheric scale (Fig. 4), similarly to findings by Brun and Beslier [42]. In this case, both rift margins display similar structural evolution and maximum thinning of the lithosphere is localised at the rift axis, which represents the centre of symmetry (e.g., [42]).

Current analogue models implement previous experimental works by considering pre-rift lateral variations in Moho topography within inherited weak zones (as mobile belts). The modelling results confirm that variations in the crustal thickness are, to a large extent, able to control the continental rifting process [12–14]. A local increase in thickness of the crust is indeed expected to greatly reduce the integrated resistance of the lithosphere by replacing the strong lithospheric mantle material with weak crustal material and increasing initial Moho temperatures (e.g., [44]), thus focusing extensional deformation. The modelling results suggest that asymmetric Mohos are prone to produce asymmetric rifting with prominent asymmetries in vertical throw on boundary faults, in the patterns of lithospheric thinning/asthenospheric upwelling and in the trajectories of magma migration. The pre-rift crustal topography, in particular, induces maximum thinning of the lithosphere to be localized at the edge of the rift zone in correspondence to the initial deepest Moho. It is here that the maximum slip occurs on the boundary faults, as well as maximum margin uplift, basin subsidence and asthenospheric upwelling.

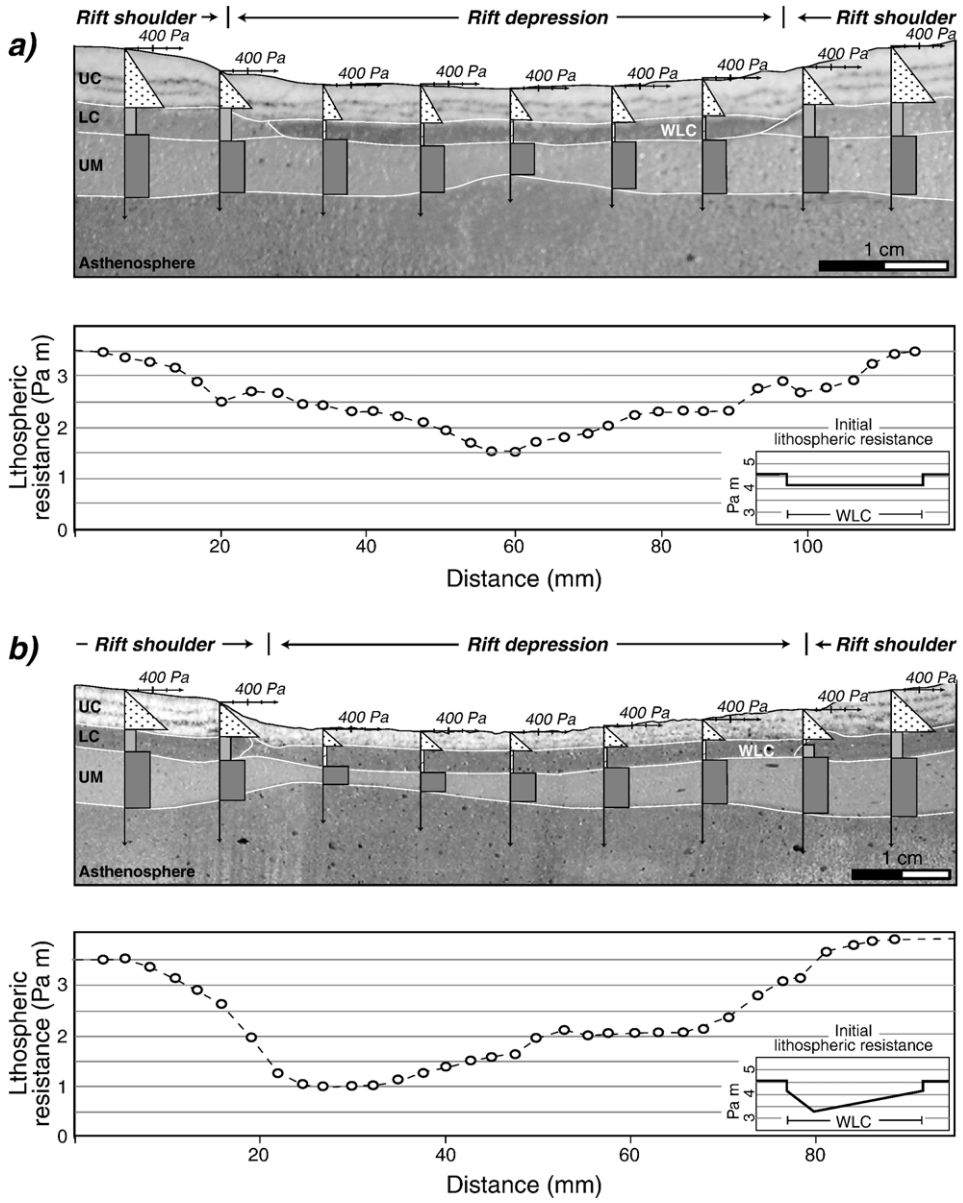

Fig. 8. Lateral variations in the mechanical strength of the experimental lithosphere of model RWZR16. a) Strength profiles calculated in different regions of the model. b) Integrated resistance of the thinned model lithosphere (calculated as the sum of the strength of the single layers); inset shows the initial resistance of the lithosphere.

Thus, although rift asymmetry has been widely used as an argument in support of simple shear kinematics, analysis of current model results suggests, on the other hand, that no major lithospheric-scale shear zones are required to produce a final asymmetric distribution of structures, supporting findings from previous analogue [42] and numerical (e.g., [24,45]) models. In the rheological conditions considered in these experiments, faulting is restricted to the upper crust and distributed ductile deformation accommodates extension in the lower crust and upper mantle. In these layers, deformation affects an area that is much wider than the rift at surface, as imaged in natural active rifts (e.g., Rio Grande) [46]; the pre-rift structure induces the laterally inhomogeneous thinning that leads to the final asymmetric configuration of lithospheric/asthenospheric extension. However, since the current models considered isotropic crustal and mantle layers, the results do not rule out the possibility that — in nature — former discontinuities due to crustal or lithospheric stacking may be re-activated during the

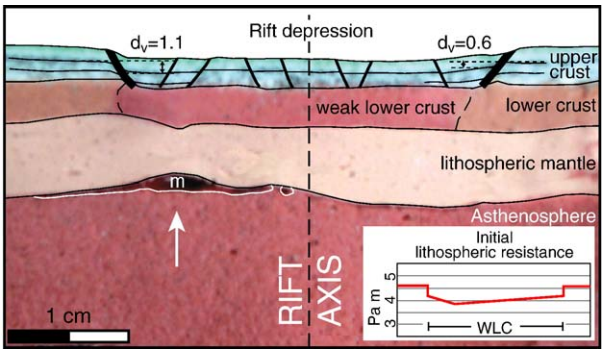

Fig. 9. Cross-section of model RWZR14 (crustal thickness: 7 mm; maximum crustal thickness: 8 mm; bulk extension: 18%; presence of sub-lithospheric melt). Inset shows the reduction in lithospheric resistance (~15%) in correspondence of the thickest WLC. White arrow indicates the area of maximum lithospheric thinning; d_v is the vertical displacement on the major boundary faults.

extensional episode leading to asymmetric deformation, as predicted by previous numerical modelling [47].

In the current models, the trajectories of the ascending magma suggest that the asymmetric evolution of rifting has a strong influence on the migration of sub-lithospheric melts. The offset lithospheric thinning alters the roughly symmetric outward magma migration suggested by previous analogue modelling [30], leading to preferential migration towards the main rift margin, close to the initial weakest area.

4.2. Development of an asymmetric passive margins pair

Asymmetric model results may provide useful insights into the process of continental break-up and subsequent formation of a pair of asymmetric passive margins. During continental rupture and the transition to oceanic spreading, the asymmetric rift is in fact expected to evolve into a conjugate passive margin pair that should retain the initial asymmetry of the rift basin. Continental

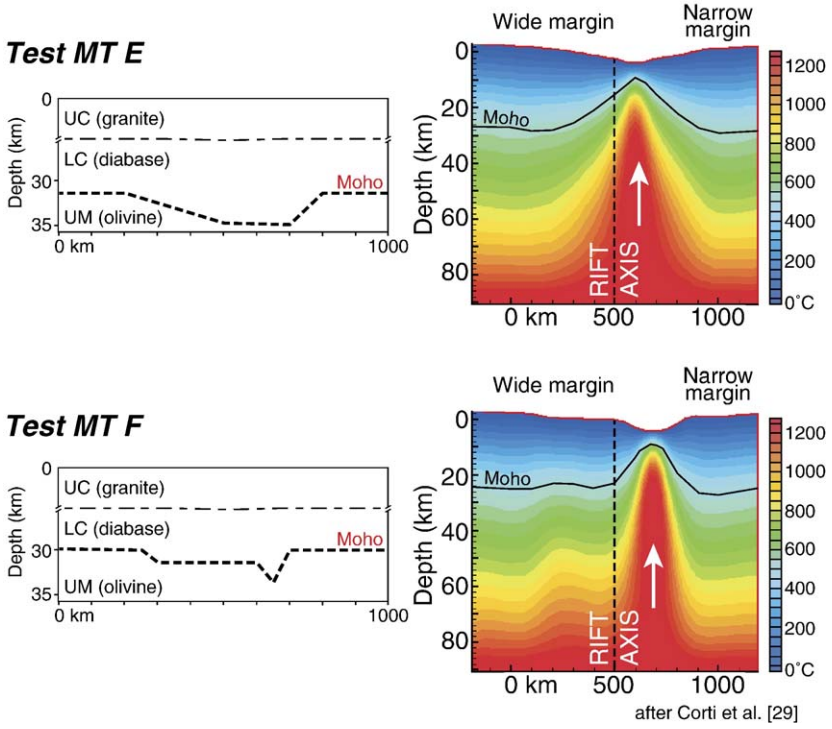

Fig. 10. Pre-rift lithosphere configuration (left panel) and thermal conditions after 12 My of stretching (right panel) for numerical models MT E and F (after [29]). See main text for details.

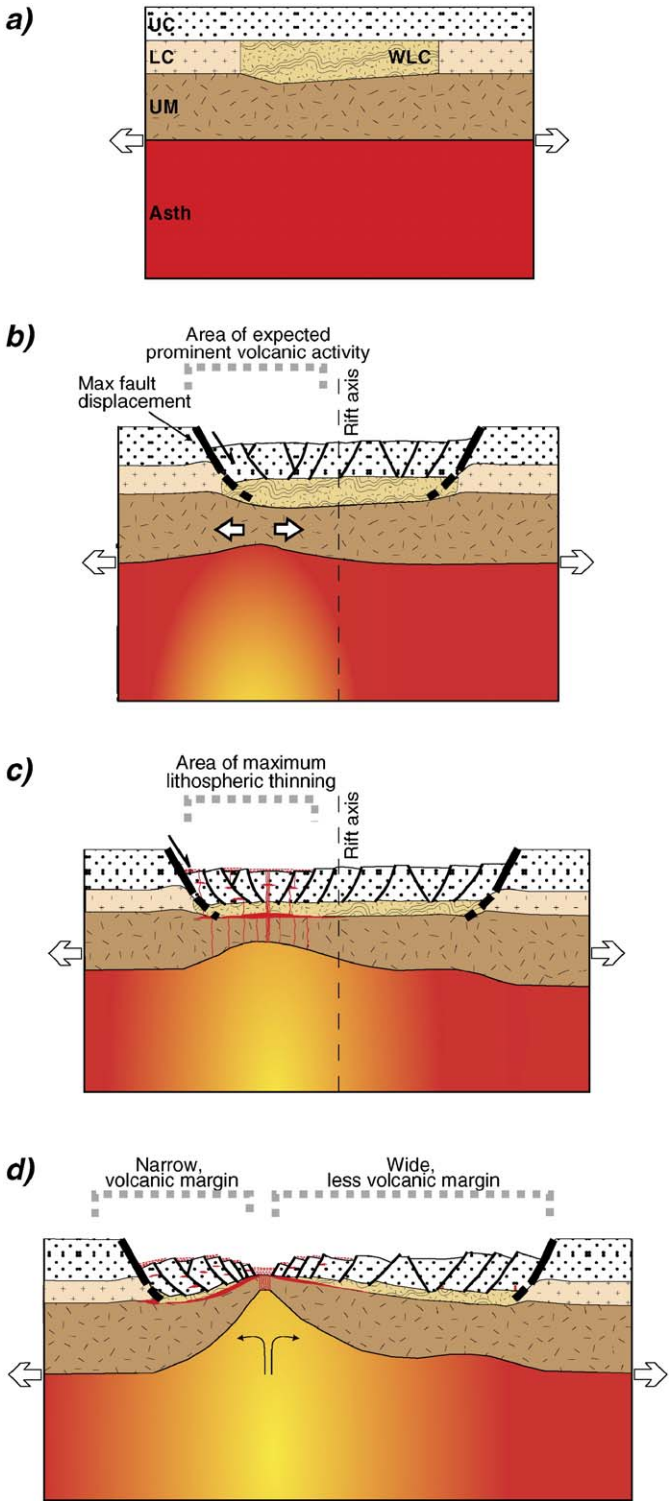

Fig. 11. Model-derived schematic evolution of lithospheric extension from continental rifting stage to formation of conjugate passive margins. a) Pre-rift lithospheric configuration. Asth: asthenosphere; LC: lower crust; UC: upper crust; UM: upper mantle; WLC: weak lower crust. b) Early continental rifting stage. The area of expected prominent volcanic activity and maximum displacement on boundary faults is indicated. c) Late continental rifting. d) Continental break-up stage with development of passive margins. Asymmetries observed in the models are extrapolated to large-scale structures of conjugate margin pair.

break-up is expected to occur in the regions of minimum strength of the extended lithosphere, close to the rift margin developing in correspondence to the initial weakest parts of models (i.e., thickest WLC). There, important thermal effects of asthenospheric upwelling and related magma-assisted processes (as intensive dyke injection) are expected to enhance strain localisation (e.g., [48]) and lead to continental break-up. This is supported by previous numerical models [29] showing that the asymmetric pre-rift Moho profiles evolve in asthenospheric upwelling located away from the rift centre, with offset break-up and final development of an asymmetric (narrow-wide) conjugate margin pair (Fig. 10). The hypothesised evolution from continental rifting to oceanization is schematically portrayed in Fig. 11. The model-derived patterns of lithospheric thinning and asthenospheric upwelling, suggest that, after termination of rifting, incipient oceanic spreading is expected to be offset with respect to the centre of the rift depression, towards the regions of thickest Moho (e.g., [13,14]). Rift asymmetry and rupture of the continental lithosphere at one side of the rifting zone produces a pair of narrow-wide conjugate margins (e.g., [4,13,24]). The narrow passive margin is characterised by a narrow zone of thinned crust, large bounding faults with high throw and maximum relative uplift of the shoulders, and a narrow continental shelf (Fig. 11). Given the asymmetric trajectories of magma migration, this margin may be the locus of important volcanic activity and strong underplating of the rift shoulders (Fig. 9). Conversely, the counterpart is expected to be a wide margin, with distributed deformation taken up by horst-and-graben structures, small throw of the bounding faults, limited basin subsidence and a broad continental shelf (Fig. 11). This margin is expected to be affected by a lesser amount of volcanism, focused in the area of transition between continental and oceanic crust.

Break-up of the continental lithosphere at the edge of the rift zone leading to development of a narrow-wide margin pair was also described in natural examples, as the Orphan Basin in the North Atlantic [24] and the conjugate margins of the Gulf of Aden [4] and Labrador Sea [1] (Figs. 1, 12). In the latter, lithospheric thinning at a rift margin was related to cooling and hardening of the central rift zone or to small-scale convection processes intensifying heating and weakening of the lithosphere (Fig. 12) [1]. Although these processes may contribute to amplifying the break-up at rift edges, the current models suggest that this type of rift evolution may simply be controlled by the pre-rift Moho profile.

The pattern of narrow-volcanic, wide-less volcanic conjugate margins is also supported in nature by the

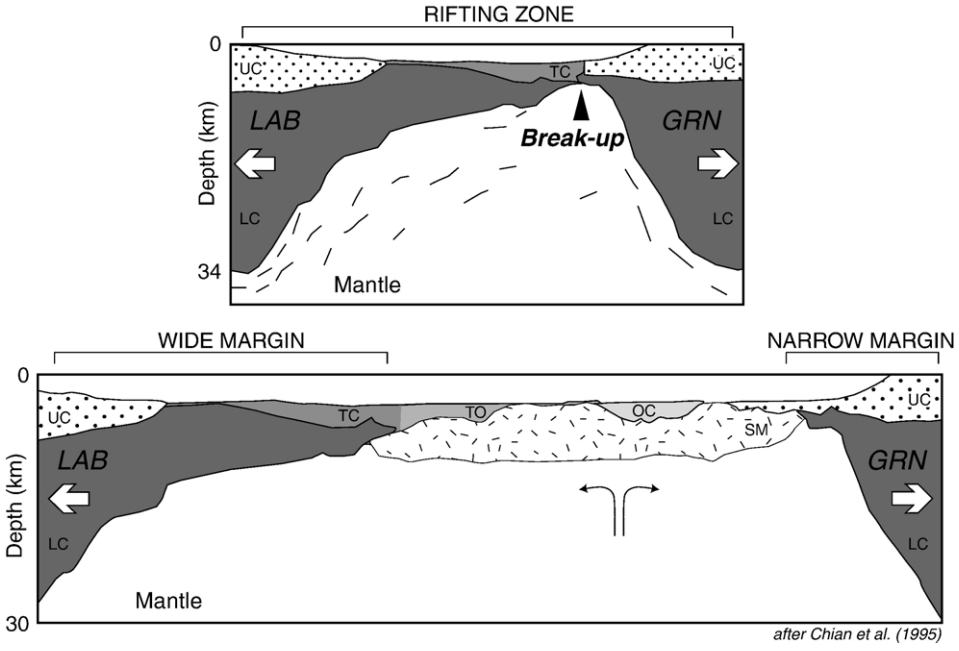

Fig. 12. Crustal reconstruction at different stages of the rifting process, showing location of continental break-up at one edge of the rifting zone and the development of an asymmetric narrow-wide margins pair. GRN: Greenland; LAB: Labrador. LC: continental lower crust; OC: oceanic crust; SM: serpentinized upper mantle; TC: transition crust of possible continental origin; TO: transition crust of possible oceanic origin; UC: continental upper crust. Modified after [1].

observation that volcanic margins are normally narrower than non-volcanic ones [19]. Moreover, the patterns of underplating described above may account for the asymmetric development of off-axis volcanism in active rifts as the Main Ethopian [49] or Kenya [50] rifts; model results can also account for the strongly asymmetric relations between doming, rifting and volcanism observed for instance in the Red Sea (e.g., [3]), where important magmatic underplating during the continental rifting stage has been hypothesised (e.g., [51]). In the Red Sea, doming is markedly asymmetric and volcanism is concentrated on the Arabian shield suggesting that the rising mantle diapir is laterally offset from the rift centre (e.g., [3]). In this case, processes such as westward drift of the lithosphere [26] or mantle megaplume upwelling beneath the Red Sea flank of the Arabian plate [52] may enhance the asymmetric patterns of uplift and magmatism.

As nature is clearly more complicated than an experimental system, the pattern of deformation recorded in continental rift systems and conjugate passive margins is expected to be more complex than that achieved in these simple analogue models. However, with the simple geometry adopted in these models, we were able to clarify the primary effects of the initial Moho topography on the rifting process and on the diversity of continental margins worldwide.

5. Conclusions

Results of scaled analogue models suggest that the pre-rift Moho topography may have a great control over the process of continental rifting. In particular, initial asymmetric Moho profiles result in strong asymmetric rifting, with prominent asymmetries in the amount of extension accommodated by boundary faults, in the patterns of lithospheric thinning/asthenospheric upwelling and in the trajectories of magma migration. During continental rupture and the transition to oceanic spreading, the asymmetric rift is expected to evolve into a pair of asymmetric passive margins, with a narrow, strongly volcanic margin and a wide, less volcanic (or with focused volcanic activity) counterpart.

Acknowledgments

The authors thank Olivier Merle and three anonymous reviewers for the constructive comments, which helped to improve the manuscript. Thanks are also due to E. Bonatti, E. Carminati and C. Doglioni for their careful reading and comments on the manuscript, and to M.H. Dickson for improving the English text. Dr. Baldi of the Colorobbia Italia S.p.A. is also gratefully acknowledged for providing the K-feldspar and corundum sands used in the experiments.

Appendix A. Supplementary data

Supplementary data associated with this article can be found, in the online version, at doi:10.1016/j.epsl.2006.02.004.

References

[1] D. Chian, C. Keen, I. Reid, K.E. Louden, Evolution of nonvolcanic rifted margins: new results from conjugate margins of the Labrador Sea, Geology 23 (1995) 589–592.
[2] J.R. Hopper, T. Funck, B.E. Tucholke, H.C. Larsen, S.W. Holbrook, K.E. Louden, D. Shillington, H. Lau, Continental breakup and the onset of ultraslow seafloor spreading off Flemish Cap on the Newfoundland rifted margin, Geology 32 (2004) 93–96.
[3] P.A. Ziegler, S.A.P.L. Cloetingh, Dynamic processes controlling evolution of rifted basins, Earth-Sci. Rev. 64 (2004) 1–50.
[4] E. d'Acremont, S. Leroy, M.-O. Beslier, N. Bellahsen, M. Fournier, C. Robin, M. Maia, P. Gente, Structure and evolution of the eastern Gulf of Aden conjugate margins from seismic reflection data, Geophys. J. Int. 160 (2005) 869–890.
[5] G.S. Lister, M.A. Etheridge, P.A. Symonds, Detachment faulting and the evolution of passive continental margins, Geology 14 (1986) 246–250.
[6] G.S. Lister, M.A. Etheridge, P.A. Symonds, Detachment models for the formation of passive continental margins, Tectonics 10 (1991) 1038–1064.
[7] D.S. Sawyer, Rifted continental margins of North America, in: R.C. Speed (Ed.), Phanerozoic Evolution of North American Continent-Ocean Transitions, Geol. Soc. Am., DNAG Continent-Ocean Transect Volume, 1994, pp. 453–476.
[8] B. Wernicke, Uniform-sense simple shear of the continental lithosphere, Can. J. Earth Sci. 32 (1985) 108–125.
[9] D. McKenzie, Some remarks on the development of sedimentary basins, Earth Planet. Sci. Lett. 40 (1978) 25–32.
[10] W.R. Buck, Modes of continental lithospheric extension, J. Geophys. Res. 96 (1991) 20161–20178.
[11] J.-P. Brun, Narrow rifts versus wide rifts: inferences for the mechanics of rifting from laboratory experiments, Philos. Trans. R. Soc. Lond., A 357 (1999) 695–712.
[12] J.A. Dunbar, D.S. Sawyer, Continental rifting at pre-existing lithospheric weaknesses, Nature 333 (1988) 450–452.
[13] J.A. Dunbar, D.S. Sawyer, How pre-existing weaknesses control the style of continental breakup, J. Geophys. Res. 94 (1989) 7278–7292.
[14] J.A. Dunbar, D.S. Sawyer, Patterns of continental extension along the conjugate margins of the central and north Atlantic oceans and Labrador Sea, Tectonics 8 (1989) 1059–1077.
[15] J. Braun, C. Beaumont, Dynamical models of the role of crustal shear zones in asymmetric continental extension, Earth Planet. Sci. Lett. 93 (1989) 405–423.
[16] D.L. Harry, D.S. Sawyer, A dynamic model of extension in the Baltimore Canyon Through region, Tectonics 8 (1992) 420–436.

[17] J.R. Hopper, R.W. Buck, The effect of lower crust flow on continental extension and passive margin formation, J. Geophys. Res. 101 (1996) 20175–20194.
[18] J.W. Van Wijk, Role of weak zone orientation in continental lithosphere extension, Geophys. Res. Lett. 32 (2005) L02303, doi:10.1029/2004GL022192.
[19] R.S. White, D. McKenzie, Magmatism at rift zones: the generation of volcanic continental margins and flood basalts, J. Geophys. Res. 94 (1989) 7685–7729.
[20] P.C. England, Constraints on extension of continental lithosphere, J. Geophys. Res. 88 (1983) 1145–1152.
[21] N.J. Kuznir, R.G. Park, The extensional strength of the continental lithosphere: its dependence on geothermal gradient, and crustal composition and thickness, in: M.P. Coward, J.F. Dewey, P.L. Hancock (Eds.), Continental Extensional Tectonics, Geol. Soc. Spec. Pub., vol. 28, 1987, pp. 35–52.
[22] L.J. Sonder, P.C. England, Effects of temperature-dependent rheology on large-scale continental extension, J. Geophys. Res. 94 (1989) 7603–7619.
[23] J.W. Van Wijk, S.A.P.L. Cloetingh, Basin migration caused by slow lithospheric extension, Earth Planet. Sci. Lett. 198 (2002) 275–288.
[24] G. Bassi, C.E. Keen, P. Potter, Contrasting styles of rifting: models and examples from the Eastern Canadian margin, Tectonics 12 (1993) 639–655.
[25] C. Doglioni, E. Carminati, E. Bonatti, Rift asymmetry and continental uplift, Tectonics 22 (2003) 1024, doi:10.1029/2002TC001459.
[26] R.S. Huismans, C. Beaumont, Symmetric and asymmetric lithospheric extension: relative effects of frictional-plastic and viscous strain softening, J. Geophys. Res. 108 (2003) 2496, doi:10.1029/2002JB002026.
[27] T.J. Reston, J. Pennel, A. Stubenrauch, I. Walker, M. Perez-Gussinye, Detachment faulting, mantle serpentinization, and serpentinite-mud volcanism beneath the Porcupine Basin, southwest of Ireland, Geology 29 (2001) 587–590.
[28] J.R. Hopper, R.W. Buck, Styles of extensional decoupling, Geology 26 (1998) 699–702.
[29] G. Corti, J. Van Wijk, M. Bonini, D. Sokoutis, S. Cloetingh, F. Innocenti, P. Manetti, Transition from continental break-up to punctiform seafloor spreading: how fast, symmetric and magmatic, Geophys. Res. Lett. 30 (2003) 1604, doi:10.1029/2003GL017374.
[30] G. Corti, M. Bonini, D. Sokoutis, F. Innocenti, P. Manetti, S. Cloetingh, G. Mulugeta, Continental rift architecture and patterns of magma migration: a dynamic analysis based on centrifuge models, Tectonics 23 (2004) TC2012, doi:10.1029/2003TC001561.
[31] J. Versfelt, B.R. Rosendahl, Relationships between pre-rift structure and rift architecture in Lakes Tanganyika and Malawi, East Africa, Nature 337 (1989) 354–357.
[32] M. Pèrez-Gussinyé, A.B. Watts, The long-term strength of Europe and its implications for plate forming processes, Nature 436 (2005) 381–384.
[33] J.F. Dewey, Diversity in the lower continental crust, in: J.B. Dawson, D.A. Carswell, J. Hall, K.H. Wedepohl (Eds.), The Nature of the Lower Continental Crust, Geol. Soc. Spec. Pub., vol. 24, 1986, pp. 71–78.
[34] C. Ebinger, N.H. Sleep, Cenozoic magmatism in central and east Africa resulting from impact of one large plume, Nature 395 (1998) 788–791.
[35] V. Courtillot, C. Jaupart, I. Manighetti, P. Tapponnier, J. Besse, On the causal links between flood basalts and continental breakup, Earth Planet. Sci. Lett. 166 (1999) 177–195.
[36] M.A. Menzies, S.L. Klemperer, C.J. Ebinger, J. Baker, Characteristics of volcanic rifted margins, in: M.A. Menzies, S.L. Klemperer, C.J. Ebinger, J. Baker (Eds.), Volcanic Rifted Margins, Geol. Soc. Am. Spec. Paper, vol. 362, 2002, pp. 1–14.
[37] G. Corti, M. Bonini, S. Conticelli, F. Innocenti, P. Manetti, D. Sokoutis, Analogue modelling of continental extension: a review focused on the relations between the patterns of deformation and the presence of magma, Earth-Sci. Rev. 63 (2003) 169–247.
[38] E. Burov, S. Cloetingh, Erosion and rift dynamics: new thermomechanical aspects of post-rift evolution of extensional basins, Earth Planet. Sci. Lett. 150 (1997) 7–26.
[39] E. Burov, A. Poliakov, Erosion and rheology controls on synrift and postrift evolution: verifying old and new ideas using a fully coupled numerical model, J. Geophys. Res. 106 (2001) 16461–16481.
[40] S. Cloetingh, P.A. Ziegler, F. Beekman, P.A.M. Andriessen, L. Matenco, G. Bada, D. Garcia-Castellanos, N. Hardebol, P. Dèzes, D. Sokoutis, Lithospheric memory, state of stress and rheology: neotectonic controls on Europe's intraplate continental topography, Quat. Sci. Rev. 24 (2005) 241–304.
[41] P. Allemand, J.-P. Brun, P. Davy, J. Van Den Driessche, Symétrie et asymétrie des rifts et mécanismes d'amincissement de la lithosphère, Bull. Soc. Géol. Fr. 8 (1989) 445–451.
[42] J.-P. Brun, M.O. Beslier, Mantle exhumation at passive margins, Earth Planet. Sci. Lett. 142 (1996) 161–173.
[43] L. Michon, O. Merle, Mode of lithospheric extension: conceptual models from analogue modeling, Tectonics 22 (2003) 1028, doi:10.1029/2002TC001435.
[44] J.C. Afonso, G. Ranalli, Crustal and mantle strengths in continental lithosphere: is the jelly sandwich model obsolete? Tectonophysics 394 (2004) 221–232.
[45] T.J. Nagel, R.W. Buck, Symmetric alternative to asymmetric rifting models, Geology 32 (2004) 937–940.
[46] D. Wilson, R. Aster, M. West, J. Ni, S. Grand, W. Gao, W.S. Baldridge, S. Semken, P. Patel, Lithospheric structure of the Rio Grande rift, Nature 433 (2005) 851–855.
[47] L. Le Pourhiet, E. Burov, I. Moretti, Rifting through stack of inhomogenous thrusts (the dipping pie concept), Tectonics 23 (2004) TC4005, doi:10.1029/2003TC001584.
[48] J.-M. Kendall, G.W. Stuart, C.J. Ebinger, I.D. Bastow, D. Keir, Magma-assisted rifting in Ethiopia, Nature 433 (2005) 146–148.
[49] M. Bonini, D. Sokoutis, G. Mulugeta, M. Boccaletti, G. Corti, F. Innocenti, P. Manetti, F. Mazzarini, Dynamics of magma emplacement in centrifuge models of continental extension with implications for flank volcanism, Tectonics 20 (2001) 1053–1065.
[50] W. Bosworth, Off-axis volcanism in the Gregory rift, east Africa: implications for models of continental rifting, Geology 15 (1987) 397–400.
[51] E. Bonatti, M. Seyler, Crustal underplating and evolution in Red Sea Rift inferred from an uplifted metagabbro/gneiss crustal complex on Zabargad island, J. Geophys. Res. 92 (1987) 12.803–12.821.
[52] A. Daradich, J.X. Mitrovica, R.N. Pysklywec, S.D. Willett, A.M. Forte, Mantle flow, dynamic topography, and rift-flank uplift of Arabia, Geology 31 (2003) 901–904.